

# A COMPARISON OF NUMERICAL MODELLING STRATEGIES IN CONTACT DETONATION SCENARIOS WITH CONCRETE TARGETS

B. ESTEBAN & N. GEBBEKEN

Institute of Engineering Mechanics and Structural Analysis, University of the Bundeswehr Munich, Germany.

## ABSTRACT

With continuous advancements in computational capacity, it has become possible and feasible to numerically model very complex physical phenomena, for instance, high dynamic loads. Hydrocodes or, in other words, “wave propagation codes” were conceived to model such scenarios. Several numerical discretisations are available in these programs, which require the problem at hand to be modelled in distinct ways and which yield different results. In the present contribution, three different numerical strategies are compared. These employ a coupling of the Euler and the Lagrange scheme, the Euler scheme by itself as well as the Smooth Particle Hydrodynamics (SPH) scheme. Their application in the hydrocode ANSYS Autodyn to a contact detonation scenario with a concrete target and with a breakthrough is described as an example of a high dynamic load. This scenario is of special interest since it is a possible threat to critical infrastructure. The numerical results are compared and contrasted; individual strengths and weaknesses of the three numerical modelling strategies are identified also by validating their numerical results with an experimental one. To the authors’ knowledge, such comparison has not yet been done for contact detonation. It is concluded that the SPH method is the preferred strategy to model the considered scenario.

*Keywords:* ANSYS Autodyn, concrete, contact detonation, damage, high dynamic loads, numerical modelling strategies, numerical simulations.

## 1 INTRODUCTION

With continuous advancements in computational capacity, numerical simulations are becoming increasingly accurate and able to represent real-life problems. Whilst the structural response under static and quasi-static loads is generally understood for conventional problems and well established guidelines exist, this is not the case within the high dynamic loading regime. This has been a topic of ongoing research, mainly in the last two decades [1–4]. In order to model high dynamic events and to analyse the high frequency response of structural components, hydrocodes or “wave propagation codes” are successfully used (e.g. [5]). They are able to capture shock wave propagations and analyse the high frequency response of structural components. Hydrocodes can be based on the finite difference method, solving differential equations which are derived from the principles of conservation of mass, energy and momentum as well as on the constitutive law of the material relating these three variables. The discretisation of these equations is performed in time and space, taking the numerical stability of the employed explicit time integration into account by considering the Courant-Friedrich-Levy condition in every time step [6]. The numerical simulations of this paper are conducted in the commercial hydrocode ANSYS

Autodyn [7]. Once a computational model is verified and validated [8], numerical simulations enable modelling a variety of loading scenarios that would be impractical and unrealistic to be conducted experimentally.

Several numerical discretisations are available in ANSYS Autodyn, which require the problem at hand to be modelled in distinct ways and which yield different results. On the one hand, previous studies show a general comparison between numerical schemes on a theoretical basis (e.g. [9-10]). On the other hand, some studies have analysed the response of structural components to specific dynamic phenomena, having been mainly focused on impact and penetration problems (e.g. [11-15]). It was shown that the choice of the numerical scheme plays a key role in obtaining accurate and computationally efficient solutions.

The application of the current contribution is a contact detonation on a concrete target (including a breakthrough). It is chosen due to the fact that these attacks are a present threat for critical infrastructure, where normal strength concrete is widely used. These numerical simulations have two major challenges. The first challenge is the high dynamic loading regime. The maximum magnitude of the strain rates associated with contact detonation events is approximately  $10^7 \text{ s}^{-1}$ , with corresponding load duration of approximately  $10\mu\text{s}$  [4, 16]. The second challenge is the complex material behaviour of the composite material concrete, which shows, for instance, a hydrostatic pressure dependency as well as a strain rate dependency. As such, numerous material models have been conceived in hydrocodes to describe the behaviour of concrete subjected to high deformations, damage, and failure (e.g. [17-22]). A material model for concrete which was especially designed for the high dynamic loading regime and implemented in ANSYS Autodyn is the RHT material model [19, 23, 24]. It has been proven to work well in a variety of high dynamic loading scenarios (e.g. [14, 25, 26]) and it is therefore used for the target material in the current contribution's numerical simulations.

This paper is structured as follows. Firstly, in Section 2 the three numerical modelling strategies that will be compared, namely the coupled Eulerian-Lagrangian, the Eulerian and the Smoothed Particle Hydrodynamics (SPH), are introduced. Secondly, Section 3 describes the complete numerical modelling of a real-life contact detonation experiment (Fig. 1) documented

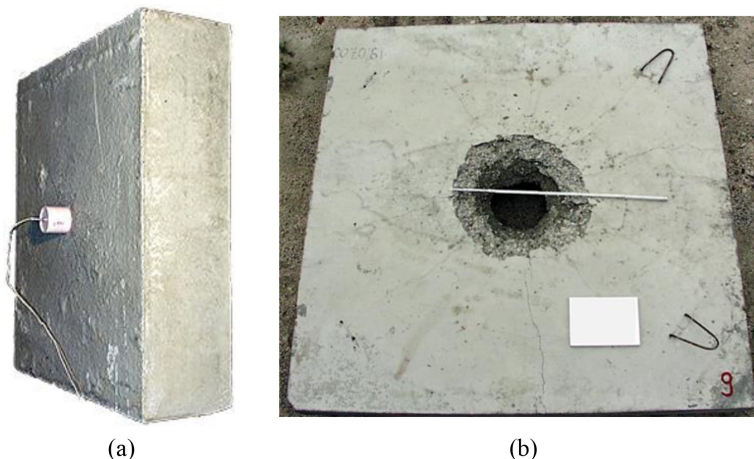


Figure 1: Contact detonation experiment: (a) frontside of concrete slab with explosive placed at the center before the experiment, (b) concrete slab after the experiment.

by Landmann [27] using the three distinct numerical schemes. Next, in Section 4 the numerical results are compared to each other (verification) and to experimental results (validation). Section 5 concludes this paper by summarising the advantages and disadvantages of the different approaches and gives a recommendation of the most suitable approach.

## 2 OVERVIEW OF THE NUMERICAL STRATEGIES

The three numerical modelling strategies that are compared in the current study are presented in Table 1. They differ in the discretisation techniques that are employed for the different material domains which are necessary for a simulation of a contact detonation problem.

### 2.1 Strategy 1: Euler-Lagrange

The first strategy is the common approach to model contact detonation problems used, for instance, in [28–31]. This classical approach models fluids in an Eulerian mesh and solids in a Lagrangian mesh. Thus, in contact detonation problems, this is translated as modelling air and explosive materials in an Eulerian mesh, where the mesh is fixed in space and the material flows through the cells. The target is modelled in a Lagrangian mesh, which means that the mesh is fixed to the material and displaces with it. Between the two mesh types, a sophisticated coupling algorithm has to be employed, which has its own computational costs. The chosen coupling algorithm in ANSYS Autodyn is the automatic (mesh free) coupling.

In its application to a contact detonation problem, this strategy faces the following challenge: in the target region close to the contact detonation, large deformations and thus mesh distortions occur, which might cause numerical instabilities. To overcome this problem, it is possible to apply an erosion criterion in ANSYS Autodyn to remove excessively distorted elements. This approach is purely numerical and has no physical meaning. The erosion criterion which is chosen in this paper uses the *instantaneous geometric strain* (GS). This scalar was introduced by ANSYS Autodyn and defined in dependency of the strain tensor as

$$\varepsilon_{GS} = \frac{2}{3} \sqrt{(\varepsilon_{11}^2 + \varepsilon_{22}^2 + \varepsilon_{33}^2) + 5(\varepsilon_{11}\varepsilon_{22} + \varepsilon_{22}\varepsilon_{33} + \varepsilon_{33}\varepsilon_{11}) - 3(\varepsilon_{12}^2 + \varepsilon_{23}^2 + \varepsilon_{31}^2)} \quad (1)$$

If this strain exceeds a certain user specified limit within an element, such element is eroded. The erosion strain limit is commonly defined by experience [31] and it is usually taken above 1.5 [12]. A disadvantage of this unphysical numerical technique is that mass and energy of eroded elements are lost. In ANSYS Autodyn, there is, however, the option to retain the inertia of eroded nodes. Nevertheless, it should be noted that the results of the numerical simulations may be very sensitive to the chosen erosion criterion [32].

Table 1: Discretisation techniques employed in the three numerical modelling strategies.

Domain (material)	Strat. 1 (Euler-Lagr.)	Strat. 2 (Euler)	Strat. 3 (SPH)
Explosive (PETN)	Euler	Euler	SPH
Target (Concrete)	Lagrange	Euler	SPH
Surrounding (Air)	Euler	Euler	Not needed

## 2.2 Strategy 2: Euler

The second strategy consists of modelling all domains in an Eulerian grid. There are two main advantages of this strategy in comparison to Strategy 1. Firstly, no coupling algorithm is necessary since there is just one discretisation type. Secondly, given that the grid is fixed in space (including for the concrete target), there are no element distortions and hence no need for an erosion criterion.

## 2.3 Strategy 3: SPH

The third strategy consists of modelling the explosive and the target using the mesh-free Smoothed Particle Hydrodynamics (SPH) method. Hereby the material is modelled as individual “particles” (interpolation points) instead of a meshed continuum like in the other mentioned discretisation techniques. Each particle has its individual material properties. They are connected by the conservation equations. A separation of the particles is, however, possible, occurring when the space between two adjacent particles exceeds a critical value. Thus, this method is capable of dealing with and capturing very large deformations without a grid tangling problem. Moreover, this feature captures fracture and fragmentation of materials, including the phenomenon of flying-off debris. Furthermore, the modelling and calculation of the surrounding air are not necessary, reducing the numerical model size. Being established fairly recently in comparison to Strategies 1 and 2, the SPH method has been proven to adequately capture material behaviour in the high dynamic loading regime (e.g. [11, 33, 34]).

## 3 NUMERICAL MODELS

In order to run numerical simulations, the following are required: geometries, discretisations, material models (target, explosive and air) and boundary conditions. Amongst these four, the greatest challenge in the problem discussed in the present paper lies in the material model due to the aforementioned complexity of concrete. Moreover, the results obtained from computational models are only as reliable as the accuracy of their input.

### 3.1 Geometry

The geometry set-up reproduces an experiment documented in [27] (Figs 1 and 2). In this experiment, the dimensions of the concrete target were  $2\text{m} \times 2\text{m} \times 0.2\text{m}$ . It was subjected to a contact detonation using a cylindrical charge of 650g of PETN 1.5 located at the geometrical centre of the target’s front side.

In order to save computational time, the experiment is modelled two-dimensional and radial symmetry is employed along the symmetry axis S.A. (Fig. 2). This numerical modification of the target’s geometry does not significantly affect the results, since the influence of the target’s corners on the localised damaged region at the centre of the target can be neglected [35].

### 3.2 Loading

The detonation (PETN) is initiated by a point located at the cylindrical charge’s face opposite to the target at the symmetry axis S.A., marked red in Fig. 2. The energy of the exploding material is transferred to the target, causing a shock wave to travel through it.

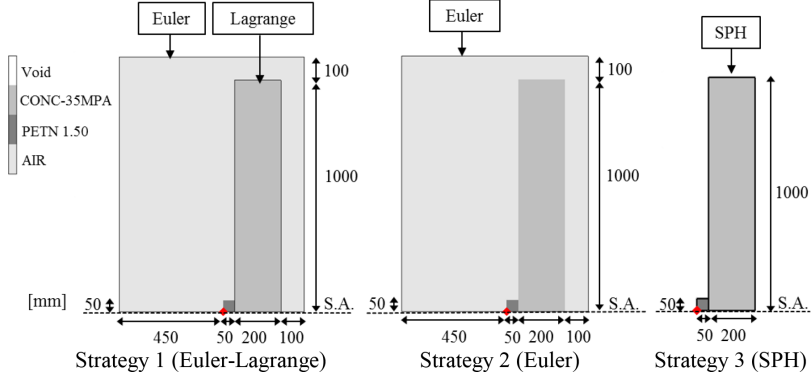


Figure 2: Contact detonation model set-up for Strategies 1 to 3, the detonation point is marked red.

### 3.3 Boundary conditions

The symmetry boundary condition is necessary for all three strategies. Further boundary conditions are just needed for Strategies 1 and 2. These are flow-out boundary conditions applied to the remaining three sides of the Euler domain. No additional boundary conditions are required for Strategy 3 since the SPH method has an infinitely large domain.

### 3.4 Material models

The material properties are taken directly from the material library of ANSYS Autodyn. A specially designed material model for concrete in the high dynamic loading regime, the RHT material model [19, 23, 24], is used for the target. Similarly to every material model in hydrocodes, the RHT separates the constitutive model into two equations. The first one, the Equation of State (EoS), relates the hydrostatic pressure of the material to its density and energy. The second one, the strength model, relates the deviatoric stresses to strain, strain rate and material damage. Stresses above a given failure surface are projected back onto it by means of a standard projection algorithm of plasticity, resulting in plastic strain increments  $\Delta\epsilon_{pl}$ . The sum of these normalised by the pressure dependent fracture strain  $\epsilon_{pl}^f(p)$  is computed over time, yielding the damage variable  $D$ ,

$$D = \sum_{\text{time steps}} \frac{\Delta\epsilon_{pl}}{\epsilon_{pl}^f(p)}. \quad (2)$$

Therefore, this damage variable considers only damage caused by the deviatoric part of the stress state. The hydrostatic part of the stress state is only regarded in the EoS and does not affect the damage variable. Other material models (e.g. [22]) define a different damage variable which combines both sources of damage.

In order to compare the numerical modelling strategies, the same material parameters are employed for all three modelling approaches. For Strategy 1, however, an erosion criterion is necessary since otherwise the simulation terminated due to large element distortions. Elements whose instantaneous geometric strain (GS) exceeds a certain threshold are eroded. This threshold is chosen to be GS = 0.05, GS = 0.5 and GS = 2 for three separate simulations in Strategy 1. No erosion criterion is necessary for Strategies 2 and 3.

### 3.5 Mesh and particle size

The discretisation should be fine enough to capture all physical phenomena and at the same time coarse enough to be computationally efficient. Therefore, the mesh size has to be determined by convergence studies, in order to make sure that the results are independent of the mesh size. For Strategies 1 and 2, a uniform mesh size of 2mm is used; for Strategy 3, a particle size of the same magnitude is chosen. The resulting number of nodes is 273,108 for Strategy 1, 221,904 for Strategy 2 and 50,625 for Strategy 3.

## 4 RESULTS

In this section, the results of five different simulations are given and compared, as shown in Table 2.

### 4.1 Run time statistics

The numerical simulation strategies are given in Table 3 together with their corresponding number of nodes, number of cycles, run time until 0.1ms and run time per cycle. As a primary analysis, the run times of the simulations until a simulation time of 0.1ms are compared. Within this simulation time, the energy of the explosion is transferred into the target (Fig. 3). The runtimes are normalised by the value of EL2.

Firstly, simulations using Strategy 1 (EL1, EL2, EL3) take significantly more time to run than using the other two strategies. This is due to the coupling algorithm between the Euler and the Lagrange domains. It decreases the time step size of the explicit time integration scheme, resulting in a larger number of cycles compared to the other two strategies. Furthermore, this

Table 2: Compared numerical simulations

Simulation	Strategy	Erosion Criterion
EL1	Strategy 1: Euler-Lagrange model	GS* = 0.05
EL2	Strategy 1: Euler-Lagrange model	GS* = 0.5
EL3	Strategy 1: Euler-Lagrange model	GS* = 2
E	Strategy 2: Euler model	-
SPH	Strategy 3: SPH model	-

\*Instantaneous Geometric Strain

Table 3: Run time statistics for the numerical modelling strategies.

Simulation	Number of Nodes	Number of Cycles Until 0.1ms [%]	Run Time Until 0.1ms [%]	Run Time Per Cycle [%]
EL1	273,108	3,198	199.2	97.7
EL2	273,108	1,568	100.0	100.0
EL3	273,108	1,539	90.5	92.2
E	221,904	576	21.7	59.1
SPH	50,625	656	11.8	28.3

coupling algorithm has its own computational costs, increasing the run time per cycle. This is clearly appreciated when comparing the run times per cycle between simulations EL and simulation E; simulations EL have 23% more nodes, however the run time per cycle is, on average (EL1, EL2, EL3), 64% larger.

Secondly, the algorithm eroding the elements requires the cycle to be recalculated. Hence, the number of cycles increases with a decreasing geometric strain limit for erosion, resulting in longer simulation run times. However, this holds only at the beginning of the simulation, since, as the simulations run longer (from  $\sim 5\text{ms}$ ), mesh distortions in the Lagrangian domain govern the time step size and therefore the total run time. This means that largely distorted elements are eroded in simulations EL1 and EL2 but such elements are retained in simulation EL3. This causes simulation EL3 to even practically stop at  $\sim 9\text{ms}$  due to the continuous decrease in time step size.

Thirdly, the SPH method is the fastest of all compared strategies mainly due to the relatively small number of nodes. This strategy employs only approximately a quarter of the nodes compared to simulations EL and E and needs approximately the same number of cycles as simulation E. However, as a mesh-free method, the SPH method comprises extra computational costs to update the region of influence of every node (and thus its magnitude of influence on a neighbouring node) for every time step. Hence, its computation time is not a quarter but rather half of the run time compared to simulation E.

#### 4.2 Transferred energy into the concrete target

In Fig. 3 the total energy in the concrete target is plotted against time. The energy transfer between the exploding material and concrete is effectively done within  $0.1\text{ms}$  in the present case scenario.

Previous studies have reported possible problems in the SPH scheme. For instance, Clegg *et al.* [12] noted problems regarding stability, consistency and conservation. In addition, Margraf [36] observed problems in the SPH scheme to release the energy of a detonation. However, the current results do not show these drawbacks due to the advances in this field. The energy resulting from the detonation which is transferred to the target has a similar order of magnitude for all employed simulations.

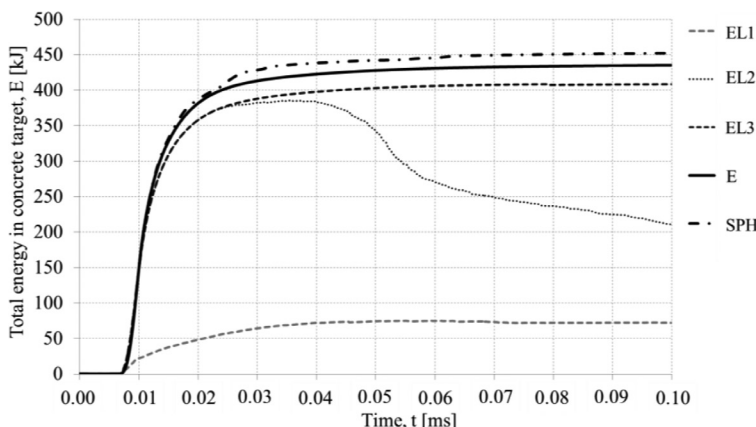


Figure 3: Variation of total energy in concrete target with time.

In simulations E and SPH, more energy is transmitted to the concrete target than in simulations EL. The reason for this is that the Euler-Lagrange coupling algorithm affects the energy transmission. Furthermore, Fig. 3 shows the effect of using different erosion criteria in simulations EL on the total energy of the target. A geometric strain erosion value of GS = 2 (EL3) does not reduce the energy in the concrete at this initial stage. With an erosion value of GS = 0.5 (EL2), the transmitted energy is reduced by the erosion of elements starting at  $\sim 0.025$ ms. Therefore, the maximum total energy transmitted to the target is just  $\sim 95\%$  of the maximum energy using the higher erosion value of GS = 2 (EL3). In addition, the total energy in the target decreases as an increasing number of elements are eroded with time. If an erosion value of GS = 0.05 (EL1) is employed, element erosion starts very early, resulting in a maximum transmitted energy of only  $\sim 20\%$  of the maximum energy using the higher erosion value of GS = 2 (EL3).

#### 4.3 Damage of concrete target

The energy transferred from the exploding material causes a shock wave in the target. The shock wave gets reflected on the backside of the target and returns as a tension wave through the concrete. This entire process can cause crater, spalling and breakthrough areas (Fig. 4). These regions are marked in Fig. 4 on a cross-section of a concrete specimen after a contact detonation experiment documented in [27].

In Fig. 5a–e, the evolution of the damage variable  $D$  at different instances of time is given for the five numerical simulations. The locality of the problem can be observed in all plots; most damage occurs within the bottom third of the target domain.

The effect of using different erosion criteria is visible in Fig. 5a–c. The simulation results vary significantly. Hence the erosion criterion choice is critical. By varying it, unphysical and arbitrary results may be achieved. However, as mentioned in Section 2.1, it is necessary to activate erosion in the Euler-Lagrange strategy. If erosion is not activated, the simulation terminates due to mesh distortions at  $\sim 0.9$ ms. This is even earlier than using a geometric strain erosion value of GS = 2 (EL3), which stops at  $\sim 9$ ms due to mesh distortions.

Using a geometric strain erosion value of GS = 0.5 (EL2), material cells which are in the direct way of the explosive charge are eroded. Since these cells correspond to material that detaches from the target and becomes debris in the current scenario, the erosion has nearly no effect on the damage of the remaining target material, where a discrete crack pattern can be observed. The crack propagation and crack direction (as produced by the shock wave) correlate well with experimental results (Table 4). With this set-up, the simulation runs until 20ms without giving numerical problems.

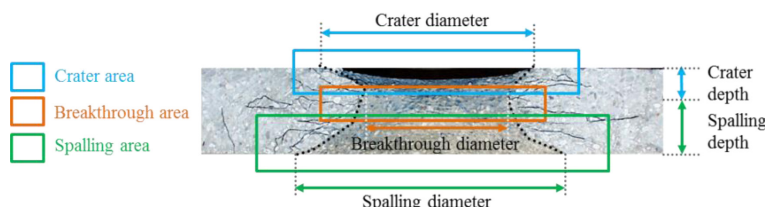


Figure 4: Cross-section of a concrete specimen after a contact detonation experiment [27], showing the definitions of crater, breakthrough and spalling areas as well as the determination of their dimensions.

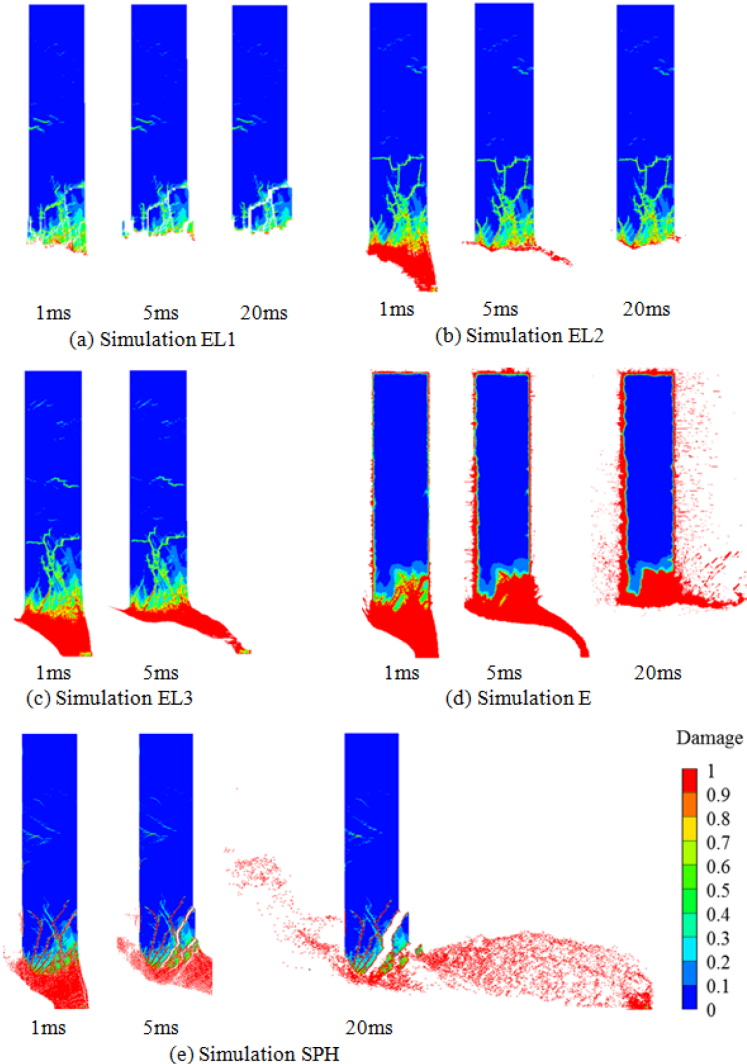


Figure 5: Evolution of damage variable at different instances of time for numerical strategies, the symmetry axis is at the base.

Further reducing the geometric strain erosion value to  $GS = 0.05$  (EL1) leads to an erosion of increasingly more material cells at the sides of the breakthrough hole. This low geometric strain erosion value leads to an erosion of most of the damaged cells, which causes material separation at the cracks. Thus, nearly no crack pattern in the inner part of the material is obtained.

The flying-off debris cannot be captured by any of the simulations EL; whilst the elements do not detach from the target in EL3 (Fig. 5c), the elements are eroded in EL1 and EL2 (Fig. 5a and b). It should be noted that in other scenarios, including contact detonation cases without a breakthrough, the erosion resulting from applying a geometric strain erosion value of  $GS = 0.5$  already has a negative effect on the results, increasing the crater dimensions unrealistically. In those scenarios, it is recommended to use a higher geometric strain erosion value.

In simulation E (Fig. 5d), the material deforms in an extensible and stretching manner, rather than in a more brittle way as would be expected in concrete. Furthermore, simulation E is not capable of capturing discrete cracks inside the material. Instead, it shows fully damaged material which remains in the target, except in the main breakthrough area. Damage appears at every interface between the target and the surrounding domain, including far away from the explosion. Moreover, target material seems to dissolve into the air. Both phenomena are unphysical and should be neglected in the further evaluation of crater and spalling dimensions. All the previously mentioned effects are due to the fact that the material simply flows through the fixed Eulerian grid and mixes at the material boundaries. The current computational set-up can be interpreted as a three fluid flow problem where the three fluids ‘air’, ‘PETN’ and ‘concrete’ move within each other and mix with each other. Despite these limitations, some flying-off debris can be seen at 20ms. Debris is, however, hard to be distinguished from the aforementioned dissolving material.

Lastly, simulation SPH (Fig. 5e) gives the most realistic representation of cracks. On the one hand, similarly to simulations EL2 and EL3, discrete crack development and propagation is present. On the other hand, it captures crack opening, as SPH particles separate. This mesh-free method is the only one, amongst the compared ones, which enables this separation. Therefore, it is the only numerical approach which adequately captures flying-off debris.

#### 4.4 Crater and spalling dimensions and their validation

The experimentally observed and the numerically simulated sizes and shapes of the target’s crater and spalling areas are compared in Table 4 and 5. After the experiments were performed, locked material was removed from the concrete target using a steel hammer [27]. This method induces the power used to remove loose material as a further aspect to bear in mind affecting the experimental damage dimensions.

In order to determine the crater and spalling dimensions of the numerical results, the damage variable needs to be interpreted. The current approach is to consider fully damaged material as material which might be locked but can, however, be easily removed by hand with a steel hammer.

Table 4 compares the crater and spalling dimensions of the numerical and experimental results. The numerical results are taken at 20ms except of EL3 where the simulation was stopped at ~9ms as discussed in Section 4.1. The cells are coloured if the numerically obtained values deviate more than 20% from the experimental values; they are coloured in orange if they are overestimated and in green if they are underestimated. The threshold of 20% has been chosen since experimental results with concrete usually have a standard deviation of up to this value [27].

The crater and spalling depths are predicted well in all simulations. Furthermore, in simulations EL, the different geometric strain limits have a noticeable impact on crater, breakthrough and spalling diameters. The lower the limit, the more elements are eroded and the higher these dimensions. Even though it seems visibly that too many elements are eroded using GS = 0.05 (EL1), this value gives the best prediction of the spalling and crater diameters amongst the simulations EL. The breakthrough diameter is, however, overestimated by 28%. The other two limits, GS = 0.5 (EL2) and GS = 2 (EL3), give fairly similar results to each other; the breakthrough diameter is correctly predicted but the spalling and crater diameters are underestimated. Since the breakthrough diameter is of major interest in a breakthrough scenario, the simulations with GS = 0.5 (EL2) and GS = 2 (EL3) are considered to be better than the simulation with GS = 0.05 (EL1). Amongst these two, the simulation

Table 4: Comparison of the crater and spalling dimensions (in cm) of the experimental and numerical results.

	Crater Diameter	Crater Depth	Break-through Diameter	Spalling Depth	Spalling Diameter
Experiment	52	8	32	12	66
EL1	50	6	41	14	75
EL2	37	7	30	13	39
EL3	34	6	29	14	38
E	47	8	42	12	61
SPH	44	7	26	13	72

EL2 is preferred since it is able to run until 20ms in the present breakthrough scenario. However, it should be noted that a variety of different geometric strain limits between 1.3 and 2 have been proven successful for other scenarios, such as impact and contact detonations without a breakthrough (e.g. [12,19,24,37,38]).

Moreover, the underestimation of the crater and spalling diameter in EL2 and EL3 could be improved if a different interpretation of the damage variable is chosen, for instance, detaching of target material is possible if the damage variable exceeds a certain threshold. This approach was proposed in [31] for their own developed material model, where the damage variable is computed differently. This approach is not employed in the present contribution (using the RHT material model) since the outcome of such procedure depends critically on the chosen threshold.

Despite the unrealistic looking dissolving effect of the target material into the air and the missing crack patterns in the target in simulation E, the crater and spalling diameters are within an acceptable range compared to the experiments. However, the breakthrough diameter is overestimated and deviates 31% from the experimental value. This is due to the fact that the shape of the breakthrough area is not a V-shape, as in the experiments and in the other simulations (Table 5), but rather tube shaped; this is created by the fluid-like flow of material.

The SPH numerical simulation is the only one whose crater and spalling dimensions lie within the 20% margin from the experiment. Therefore, it can be concluded that this particle method is the best approach to obtain accurate crater and spalling dimensions in the scenario considered in this paper.

Table 5 shows the cross-section of the experimental target in comparison to the numerical results of EL2 (the preferred one amongst the Strategy 1 simulations), E and SPH at 20ms.

#### 4.5 Summarised comparison

A summary of the findings of the three numerical modelling strategies is presented in Table 6. The three numerical strategies are compared in terms of the necessary time to set up a model, the necessary time to modify a model (e.g. to conduct a mesh convergence analysis or a parameter study), the required domains, and the quality in the prediction of damaged regions using the results of EL2 for the Euler-Lagrange Strategy as in Table 5. A tick (✓) states that the value is acceptably close to the experimental result, i.e. it differs less than 20%. A cross (✗) indicates a deviation larger than 20%.

Table 5: Cross-section of the experimental target in comparison to the numerical results at 20ms.

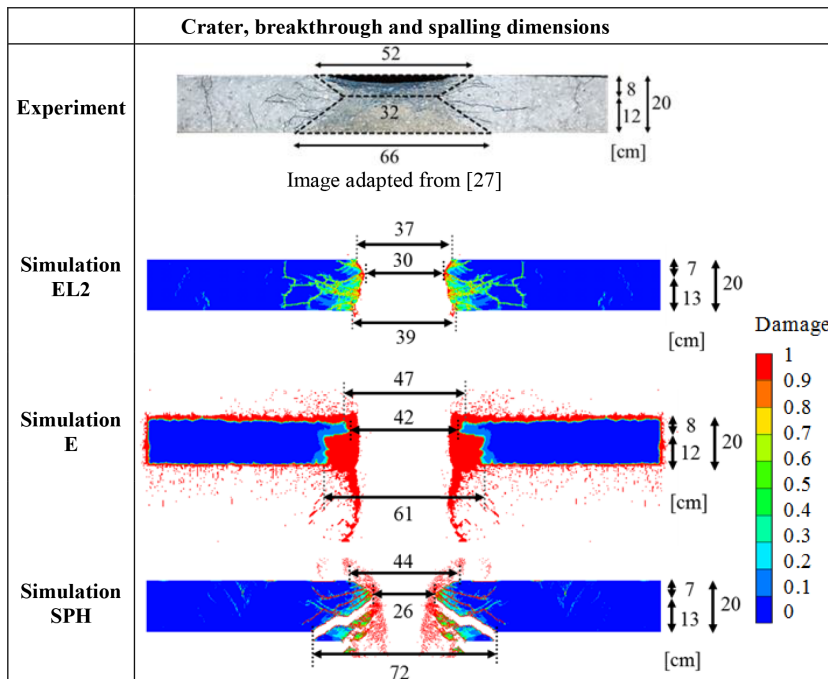


Table 6: Summary of the findings of the three numerical modelling strategies.

	Numerical modelling strategy		
	Euler-Lagrange (EL2)	Euler (E)	SPH (SPH)
<b>Time to set up model</b>	High	Medium	Low
<b>Time to modify model</b>	High	Medium	Low
<b>Required domains</b>	- Explosive - Target - Surrounding	- Explosive - Target - Surrounding	- Explosive - Target
<b>Quality in the prediction of damaged regions</b>			
• Crater depth	✓	✓	✓
• Crater diameter	✗	✓	✓
• Breakthrough diameter	✓	✗	✓
• Spalling depth	✓	✓	✓
• Spalling diameter	✗	✓	✓
• Flying-off debris	✗	✗	✓

	Numerical modelling strategy		
	Euler-Lagrange (EL2)	Euler (E)	SPH (SPH)
Further comments	Erosion criteria necessary due to mesh distortions	- Unphysical damage in target-air interface - No crack pattern inside target	



Figure 6: Superposition of the experimental and the numerical results using the SPH method as the best numerical strategy.

## 5 CONCLUSIONS

In the present contribution the strengths and weaknesses of three numerical modelling strategies are compared for a contact detonation scenario with a concrete target (including a breakthrough). It is shown that the modelling technique has a large influence on the numerical simulation results. For the presented scenario, the SPH scheme is preferred due to the following reasons. Firstly, no erosion criterion (an unphysical numerical technique) is necessary for SPH. Secondly, damaged areas are accurately captured: a realistic crack pattern inside the concrete target as well as crater and spalling dimensions. Thirdly, the SPH strategy is the computationally most efficient one. Fourthly, the SPH scheme has the advantage that flying-off debris can be modelled. This is of particular interest since high velocity debris could damage people and valuable equipment on the protective side of concrete structures. Fig. 6 shows the superposition of the experimental and the numerical results using the SPH method as the best numerical strategy.

Within the field of contact detonations, further investigations should focus on whether the findings of this paper could be extrapolated to firstly, contact detonation problems without breakthrough; secondly, 3D models of such problems; thirdly, to other target materials including reinforced concrete; and fourthly, to multi-layered targets. Moreover, the SPH technique should be further investigated for other scenarios in the high dynamic loading regime. Furthermore, the most successful interpretation of the damage variables in different material models should be investigated.

## ACKNOWLEDGEMENTS

The presented project was funded by the German Federal Ministry of Economic Affairs and Energy (BMWi) on the basis of a decision by the German Bundestag.

## REFERENCES

- [1] Bischoff, P.H. & Perry, S.H., Compressive behaviour of concrete at high strain-rates. *Materials and Structures*, **24**, pp. 425–450, 1991.  
<http://dx.doi.org/10.1007/BF02472016>
- [2] Meyers, M.A., *Dynamic Behaviour of Materials*, Wiley-Interscience: New York, 1994.  
<http://dx.doi.org/10.1002/9780470172278>
- [3] Gebbeken, N. & Ruppert, M., On the safety and reliability of hydrocode simulations. *International Journal for Numerical Methods in Engineering*, **46**, pp. 839–851, 1999.  
[http://dx.doi.org/10.1002/\(SICI\)1097-0207\(19991030\)46:6<839::AID-NME728>3.0.CO;2-R](http://dx.doi.org/10.1002/(SICI)1097-0207(19991030)46:6<839::AID-NME728>3.0.CO;2-R)
- [4] Riedel, W. & Forquin, P., Modelling the response of concrete structures to dynamic loading, (Chapter 5). *Understanding the Tensile Properties of Concrete*, ed. J. Weerheijm, Woodhead Publishing, Oxford, 2013.
- [5] Zukas, J.A., *Introduction to Hydrocodes*, Elsevier: The Netherlands, 2004.
- [6] Courant, R., Friedrichs, K. & Lewy, H., Über die partiellen Differenzengleichungen der mathematischen Physik. *Mathematische Annalen*, **100**, pp. 32–74, 1928.  
<http://dx.doi.org/10.1007/BF01448839>
- [7] ANSYS Autodyn, AUTODYN Explicit Software for Nonlinear Dynamics, *User's Manual*, Release 14.5, 2013.
- [8] American Society of Mechanical Engineers (ASME) Standards Committee on Verification and Validation in Computational Solid Mechanics (PTC 60 / V&V 10), *Guide for Verification and Validation in Computational Solid Mechanics*, ASME, 2006.
- [9] Katayama, M., Aizawa, T. & Obata, H., Lagrange, ALE and Euler Processors in AUTODYN-2D: Evaluation of Reliability through Benchmark Problems, *IMPACT III, Post Seminar of 10th International Conference on Structural Mechanics in Reactor Technology*, 1989.
- [10] Birnbaum, N.K. & Cowler, M.S., Comparison of Euler, Lagrange, ALE and coupled Euler Lagrange calculations in terminal ballistics. *Proceeding of the 11th International Symposium on Ballistics*, Vol. 2: Warhead mechanisms, terminal ballistics, 1989.
- [11] Hiermaier, S., *Numerische Simulation von Impaktvorgängen mit einer netzfreien Lagrangenmethode (Smooth Particle Hydrodynamics)*, Doctoral Thesis (in German), Institut für Mechanik und Statik, Universität der Bundeswehr München, 1996.
- [12] Clegg, R.A., Sheridan, J., Hayhurst, C.J. & Francis, N.J., The application of SPH techniques in AUTODYN-2D to kinetic energy penetrator impacts on multi-layered soil and concrete targets. *Proceeding of the 8th International Symposium on Interaction of the Effects of Munitions with Structures*, 1997.
- [13] Meuric, O.F.J., Sheridan, J., O'Carroll, C., Clegg, R.A. & Hayhurst, C.J., Numerical prediction of penetration into reinforced concrete using a combined grid based and meshless lagrangian approach. *Proceeding of the 10th International Symposium on Interaction of the Effects of Munitions with Structures*, 2001.
- [14] Leppänen, J., *Concrete Structures Subjected to Fragment Impacts*, Doctoral Thesis, Chalmers University of Technology, Göteborg, Sweden, 2004.
- [15] Gebbeken, N., Teich, M. & Linse, T., Numerical modelling of high speed impact and penetration into concrete structures. *Proceeding of the 7th International Conference on Shock & Impact Loads on Structures*, eds. F.L. Huang, Q.M. Li & T.S. Lok, CI-Premier Pte Ltd, pp. 241–250, 2007.
- [16] Gebbeken, N. & Ruppert, M., Ein Beitrag zur Simulation von Baustrukturen unter hochdynamischen Kurzzeitbeanspruchungen. *Bauingenieur*, **11**, pp. 461–470, 1999.

- [17] Holmquist, T.J. & Johnson, G.R., A computational constitutive model for concrete subjected to large strains, high strain rates, and high pressures. *Proceeding of the 14th International Symposium on Ballistics*, pp. 591–600, 1993.
- [18] Malvar, L.J., Crawford, J.E. & Wesevich, J.W., A plasticity concrete material model for Dyna3D. *International Journal of Impact Engineering*, **19**, pp. 847–873, 1997.  
[http://dx.doi.org/10.1016/S0734-743X\(97\)00023-7](http://dx.doi.org/10.1016/S0734-743X(97)00023-7)
- [19] Riedel, W., Thoma, K., Hiermaier, S. & Schmolinske, E., Penetration of reinforced concrete by BETA-B-500, numerical analysis using a new macroscopic concrete model for hydrocodes. *Proceeding of the 9th International Symposium on the Interaction of the Effects of Munitions with Structures*, pp. 318–325, 1999.
- [20] Itoh, M., Katayama, M., Mitake, S., Niwa, N., Beppu, M. & Ishikawa, N., Numerical study on impulsive local damage of reinforced concrete structures by a sophisticated constitutive and failure model. *Proceeding of the International Conference on Structures Under Shock and Impact*, pp. 569–578, 2000.
- [21] Gebbeken, N. & Ruppert, M., A new material model for concrete in high-dynamic hydrocode simulations. *Archive of Applied Mechanics*, **70**, pp. 463–478, 2000.  
<http://dx.doi.org/10.1007/s004190000079>
- [22] Hartmann, T., Pietzsch, A. & Gebbeken, N., A hydrocode material model for concrete. *International Journal of Protective Structures*, **1**, pp. 443–468, 2010.  
<http://dx.doi.org/10.1260/2041-4196.1.4.443>
- [23] Riedel, W., *Beton unter dynamischen Lasten, Meso- und makromechanische Modelle und ihre Parameter*, Doctoral Thesis (in German), Fraunhofer-Institut für Kurzzeitdynamik, Ernst-Mach-Institute EMI, Fraunhofer IRB Verlag, 2004.
- [24] Riedel, W., Kawai, N. & Kondo, K., Numerical assessment for impact strength measurements in concrete materials. *International Journal of Impact Engineering*, **36**, pp. 283–293, 2009.  
<http://dx.doi.org/10.1016/j.ijimpeng.2007.12.012>
- [25] Schuler, H. & Hansson, H., Fracture behaviour of high performance concrete (HPC) investigated with a Hopkinson-Bar. *Journal de Physique IV France*, **134**, pp. 1145–1151, 2006.  
<http://dx.doi.org/10.1051/jp4:2006134175>
- [26] Hansson, H. & Malm, R., Non-linear finite element analysis of deep penetration in unreinforced and reinforced concrete. *Nordic Concrete Research*, **44**, pp. 87–107, 2011.
- [27] Landmann, F., *Dokumentation der Parameteruntersuchungen des Schädigungsverhaltens von Stahlbetonplatten unter Kontaktdetonationen*, Technical report, Wehrtechnische Dienststelle für Schutz- und Sondertechnik, Oberjettenberg, 2001.
- [28] Kraus, D., Roetzer, J. & Thoma, K., Effect of high explosive detonations on concrete structures. *Nuclear Engineering and Design*, **150**, pp. 309–314, 1994.  
[http://dx.doi.org/10.1016/0029-5493\(94\)90149-X](http://dx.doi.org/10.1016/0029-5493(94)90149-X)
- [29] Zhou, X.Q. & Hao, H., Mesoscale modelling and analysis of damage and fragmentation of concrete slab under contact detonation. *International Journal of Impact Engineering*, **36**, pp. 1315–1326, 2009.  
<http://dx.doi.org/10.1016/j.ijimpeng.2009.02.010>
- [30] Riedel, W., Mayrhofer, C., Thoma, K. & Stolz, A., Engineering and numerical tools for explosion protection of reinforced concrete. *International Journal of Protective Structures*, **1**, pp. 85–102, 2010.  
<http://dx.doi.org/10.1260/2041-4196.1.1.85>

- [31] Hartmann, T., Pietzsch, A. & Gebbeken, N., A Hydrocode material model for concrete. *International Journal of Protective Structures*, **1**(4), pp. 443–468, 2010.  
<http://dx.doi.org/10.1260/2041-4196.1.4.443>
- [32] Luccioni, B.M., Araoz, G.F. & Labanda, N.A., Defining erosion limit for concrete. *International Journal of Protective Structures*, **4**, pp. 315–340, 2013.  
<http://dx.doi.org/10.1260/2041-4196.4.3.315>
- [33] Liu, G.R. & Liu, M.B., *Smoothed Particle Hydrodynamics - A Meshfree Particle Method*, World Scientific: Singapore, 2003.  
<http://dx.doi.org/10.1142/9789812564405>
- [34] Feng, D.L., Liu, M.B., Li, H.Q. & Liu, G.R., Smoothed particle hydrodynamics modeling of linear shaped charge with jet formation and penetration effects. *Computers & Fluids*, **86**, pp. 77–85, 2013.  
<http://dx.doi.org/10.1016/j.compfluid.2013.06.033>
- [35] Gebbeken, N. & Greulich, S., *Verhalten von Baustrukturen aus Stahlbeton unter Kontaktdetonationen: Simulationsmodell für bewehrten Beton*, Technical report, University of the Bundeswehr Munich, 2001.
- [36] Margraf, J., *Modeling the Structural Response from a Propagating High Explosive Using Smooth Particle Hydrodynamics*, Lawrence Livermore National Laboratory, Report LLNL-TR-561181, 2012.
- [37] Leppänen, J., Concrete subjected to projectile and fragment impacts: modelling of crack softening and strain rate dependency in tension. *International Journal of Impact Engineering*, **32**, pp. 1828–1841, 2006.  
<http://dx.doi.org/10.1016/j.ijimpeng.2005.06.005>
- [38] Hansson, H., *Warhead penetration in concrete protective structures*, Licentiate Thesis, School of Architecture and the Built Environment, Stockholm: Sweden, 2011.